

Combined effects of elevated temperatures and high strain rates on compressive performance of S30408 austenitic stainless steel

Li, Lijun; Wang, Rui; Zhao, Hui; Zhang, Haoran; Yan, Rui

DOI

[10.1016/j.istruc.2021.07.063](https://doi.org/10.1016/j.istruc.2021.07.063)

Publication date

2021

Document Version

Accepted author manuscript

Published in

Structures

Citation (APA)

Li, L., Wang, R., Zhao, H., Zhang, H., & Yan, R. (2021). Combined effects of elevated temperatures and high strain rates on compressive performance of S30408 austenitic stainless steel. *Structures*, 34, 1-9. <https://doi.org/10.1016/j.istruc.2021.07.063>

Important note

To cite this publication, please use the final published version (if applicable). Please check the document version above.

Copyright

Other than for strictly personal use, it is not permitted to download, forward or distribute the text or part of it, without the consent of the author(s) and/or copyright holder(s), unless the work is under an open content license such as Creative Commons.

Takedown policy

Please contact us and provide details if you believe this document breaches copyrights. We will remove access to the work immediately and investigate your claim.

1 **Combined effects of elevated temperatures and high strain**
2 **rates on compressive performance of S30408 austenitic**
3 **stainless steel**

4 Lijun Li ^a, Rui Wang ^a, Hui Zhao ^{a, b*}, Haoran Zhang ^a, Rui Yan ^c

5 *Submitted to: Structures*

6 ^aCollege of Civil Engineering, Taiyuan University of Technology, Taiyuan, China;

7 ^bDepartment of Civil Engineering, Tianjin University, Tianjin, China;

8 ^cFaculty of Civil Engineering and Geosciences, Delft University of Technology,
9 Netherlands

10 _____

11 * Corresponding author:

12 Hui Zhao

13 Tel: +86 351 6010280

14 Email: zhaohui01@tyut.edu.cn

15

16

17

18

19

20

21

22

23

24

25

26

27

28

29

30

31 **Abstract:**

32 304 austenitic stainless steel (ASS) has been increasingly utilized in engineering
33 structures. However, the lack of study on this type of steel under extreme conditions
34 restricts its application. Hence, this paper presents an experimental investigation of
35 the combined influences of elevated temperatures and high strain rates on the
36 mechanical performance of S30408 ASS, which is essential for determining the
37 behaviour of structures made with this type of steel subjected to the coupled fire and
38 impact/explosion. For this purpose, the quasi-static and dynamic compression tests
39 using Split Hopkinson Pressure Bar (SHPB) were conducted under temperatures of
40 20-600 °C and strain rates from 0.001 to 3000 s⁻¹. In addition, the corresponding
41 microstructures of tested samples were observed. The stress-strain responses, strain
42 rate and temperature effects as well as the microstructural evolutions were analyzed.
43 Test results show that the stress-strain responses are sensitive to the strain rate and
44 temperature. The strain-rate sensitivity coefficient increases as the strain rate and
45 temperature rise. The microstructural observation reveals that the grain dimension
46 declines with an increment of strain rate or a decreasing temperature. Finally, the
47 dynamic compressive stress-strain models for S30408 ASS under elevated
48 temperatures were suggested on the basis of the Johnson-Cook (J-C) model and have
49 been proved to give a reasonable prediction.

50 *Keywords:* S30408 austenitic stainless steel; Elevated temperatures; Dynamic
51 response; Strain rate; Constitutive model.

52 **1. Introduction**

53 In the last decades, 304 austenitic stainless steel (ASS) has been increasingly used in
54 engineering structures [1-6]. It has several advantages compared to carbon steel, such
55 as high corrosion resistance and durability, maintenance, improved fire and
56 impact/blast resistance, etc. Due to these benefits, it is expected to be widely
57 employed in the modern construction field, especially considering the life-cycle cost.
58 Several design codes have been developed to regulate the use of the stainless steel in
59 civil engineering, such as CECS 410:2015 [7] and EN 1993-1-4 [8]. Until now, the
60 material and structural behaviours of 304 ASS subjected to the single static, dynamic,
61 cyclic and fire conditions are relatively well understood [1-6, 9-20]. In addition to the
62 loading conditions mentioned above, the structures may suffer combined fire and
63 impact/explosion action during the lifetime [21, 22], such as 9.11 terrorist attack and
64 Qingdao pipeline leak explosion. The fire may easily results in an explosion or
65 progressive collapse, as presented in Fig. 1. Therefore, it is essential to systematically
66 investigate the mechanical performance and microstructural characteristic of 304 ASS
67 exposed to both high temperatures and strain rates in order to ensure the safety of 304
68 ASS structures subjected to such harsh environment.

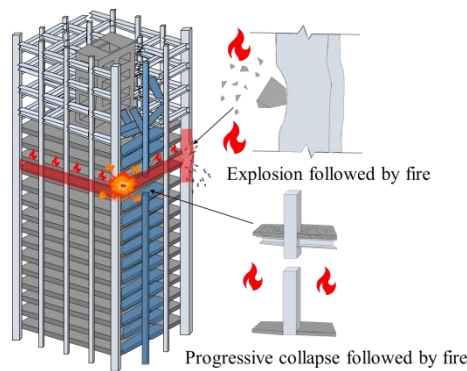


Fig. 1. Schematic view of explosion or progressive collapse followed by a fire.

69 For 304 ASS, the quasi-static mechanical performance at elevated temperatures and
70 the dynamic mechanical properties at ambient temperature have been extensively
71 examined [9, 10, 16, 18]. Results demonstrate that temperature causes a significant
72 decrease in material strength, whereas the high strain rate induces a strengthening
73 effect on the yield stress at ambient temperature. EN 1993-1-2 [23] suggests that the

74 nominal yield stress declines by about 50% when the temperature reaches 600°C.
75 Compared to carbon steel, stainless steel presents better high-temperature
76 performance. As for the effect of strain rate at ambient temperature, a pronounced
77 increase in the nominal yield stress exists provided that the strain rates exceed 10^3 s^{-1} ,
78 owing to an enhanced rate of dislocation generation. Jia et al. [18] found that the
79 dynamic yield strength of S30408 ASS under strain rate of 6212 s^{-1} can reach up to
80 approximate 3 times of that under quasi-static load.

81 Current results indicate that the mechanical properties of stainless steel are
82 temperature and strain rate sensitive. Given the coupled temperature and dynamic
83 loadings, the strengthening induced by the high strain rate and the thermal softening
84 may complicate the stress-strain responses. Though previous researches on the 304
85 ASS have covered material and structural levels, the information on the coupled
86 influences of high strain rates and elevated temperatures is still limited. Lee et al. [24,
87 25] investigated the compressive performance and microstructure change of 304L
88 ASS considering the influences of strain rate, temperature and pre-strain. Test strain
89 rates and temperatures were set in the range of $2000\text{-}6000 \text{ s}^{-1}$ and $300\text{-}800 \text{ }^\circ\text{C}$,
90 respectively. It is concluded that the strain-rate sensitivity increases with rising strain
91 rates and the descending temperatures. The microstructural observation indicated that
92 the change in the flow stress under combined high strain rates and temperatures is
93 related to the quantity of martensite and the densities of both dislocation and twin.

94 Cadoni and Forni [26] studied the influences of strain rate and temperature on the
95 mechanical responses of cold-formed AISI 304 ASS bars. Experiments were
96 conducted using a split-Hopkinson tension bar under temperatures up to $1000 \text{ }^\circ\text{C}$ and
97 3 strain rates ($250, 400$ and 800 s^{-1}). They found that the yield stress decreases with
98 the increasing temperatures and increases with an increment of the strain rate. Finally,
99 the parameters of the Johnson-Cook (J-C) and Cowper-Symonds (C-S) models were
100 determined. In 2020, Yang et al. [27] conducted SHPB tests to analyze the influences
101 of strain rate and temperature on the compressive performance of ASTM

102 A240/A240M 304 stainless steel. Due to the increased carbon content, the quasi-static
 103 yield stress achieves 702 MPa at room temperature. Additionally, the modified J-C
 104 model was suggested according to the test results. Table 1 summarizes the detailed
 105 information in literatures [24-27]. As mentioned previously, the existing researches
 106 are not sufficient to fully understand the performance of 304 ASS under combined
 107 high temperatures and high strain-rate conditions because of the different chemical
 108 compositions and test conditions.

109 **Table 1**

110 Detail information in literatures [24-27].

Sources	Type	Strain rate (s ⁻¹)	Temperature (°C)	Content
Lee et al. [24, 25]	Pre-strained 304L ASS bars	2000-4000, 4000-6000	300, 500, 800	Compressive stress-strain curves, microstructure
Cadoni and Forni [26]	AISI304 ASS bars in cold forming	250, 400, 800	200, 400, 600, 800, 1000	Tensile stress-strain curves, constitutive models
Yan et al. [27]	ASTM A240/A240M 304 ASS	1000, 3000, 5000	300, 500, 700	Compressive stress-strain curves, constitutive models

111 In this context, the quasi-static and dynamic compressive behaviours of a typical 304
 112 ASS have been investigated under varying high temperatures (from 20 to 600 °C) and
 113 strain rates (0.001, 1000, 2000 and 3000 s⁻¹). The universal compression machine and
 114 SHPB tester equipped with an electric furnace were employed for the quasi-static and
 115 dynamic tests under elevated temperatures, respectively. The stress-strain responses,
 116 strain rate and temperature effects and microstructural changes were obtained and
 117 analyzed. Finally, the dynamic stress-strain model considering both the temperature
 118 and strain rate is developed on the basis of the J-C model. The above results can be
 119 used for evaluation of the structural safety when subjected an impact/explosion
 120 followed by a fire.

121 **2. Experiments**

122 **2.1. Material and Sample preparation**

123 The material investigated in this work was S30408 ASS with the following chemical
 124 composition: C(0.02%), S(0.002%), P (0.033%), Si(0.46%), Mn(1.35%), Cr(18.15%),
 125 Ni(8.06%), corresponding to 304 in ASTM [28] and 1.4301 in EN 10088-1 [29]. All
 126 samples for mechanical characterization were obtained from the steel tube in the

127 longitudinal direction using the wire-cut electrical discharge machine. In order to
128 achieve good flatness and parallelism, the ends of SHPB samples were polished using
129 a series of sand papers (grit dimensions: 400 to 2000 mesh). The quasi-static tensile
130 test was conducted at room temperature with a constant 0.001 s^{-1} strain rate, according
131 to ISO 377:2013 [30]. The engineering stress-strain relationships are depicted in Fig.
132 2. Due to the unobvious yield plateau, the yield stress was taken as the 0.2% proof
133 stress in accordance with GB/T 228.1-2010 [31]. The mean Young's modulus, yield
134 strength, ultimate tensile strength and elongation are 191.4 GPa, 261.3 MPa, 611.2
135 MPa and 54%, respectively. According to GB/T 34108-2017 [32], samples for
136 quasi-static and dynamic compression tests under elevated temperatures are
137 cylindrical in shape with dimensions of $\varnothing 5 \text{ mm} \times 5 \text{ mm}$ and $\varnothing 8 \text{ mm} \times 4 \text{ mm}$,
138 respectively. A diameter to height ratio of 2 is designed in the dynamic compression
139 samples to decrease the influences of friction and inertia.

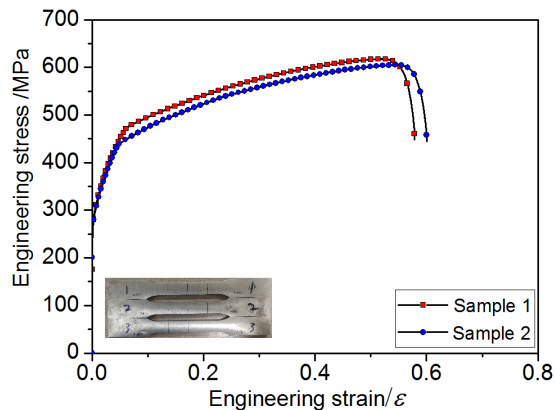


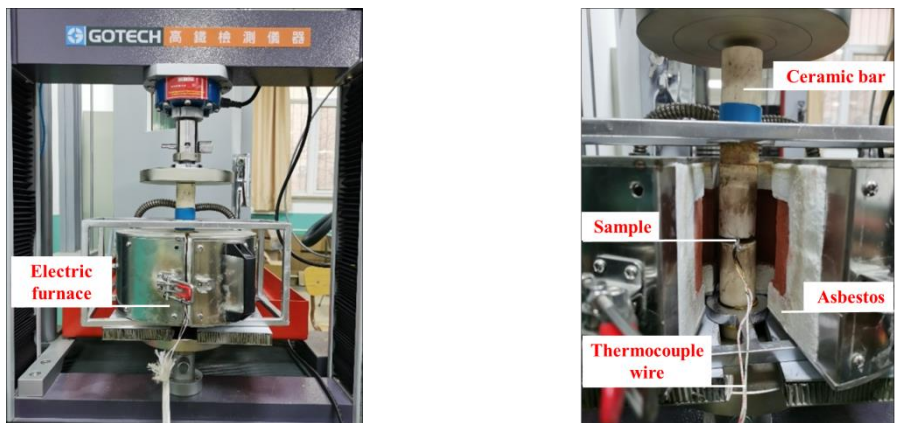
Fig. 2. Stress-strain responses of S30408 ASS under quasi-static tensile.

140 2.2. Experimental setup and procedure

141 2.2.1 Quasi-static compression under elevated temperatures

142 A quasi-static compression test can serve as a basis for assessing the thermal and
143 strain-rate effects. A total of 12 samples were tested in a quasi-static compression
144 regime using a 30 kN universal compression machine equipped with an electric
145 furnace, as presented in Fig. 3. Two high-temperature resistance and high strength
146 ceramic bars were installed to transfer the load from the testing machine to the sample.
147 The thermocouple wire was wrapped around the sample to monitor the temperature.

148 Samples were first heated to the target temperatures (200, 400 and 600 °C) with the
149 speed of 2 °C/min. Then, in order to ensure a homogenous temperature within the
150 samples, the target temperatures were held for 5 min. Finally, the samples were
151 compressed with the rate of 0.3 mm/min to failure in a steady-state condition. The
152 corresponding load and deformation were automatically obtained. At least three tests
153 were performed for each strain rate and temperature, and final results were the
154 average value of three samples.



(a) Whole apparatus (b) Internal state of the furnace
Fig. 3. Device for Quasi-static compression at elevated temperatures.

155 2.2.2 Dynamic test under elevated temperatures

156 It is known that the SHPB device is the most widely used to measure the dynamic
157 mechanical properties of steel material. In this work, 36 dynamic tests were
158 performed using an SHPB tester accompanying an electric oven with a 1200 °C
159 heating capacity. The equipment contains the air gun, strike, incident and transmitter
160 bars, an energy-absorption apparatus and an oven. The photo and schematic view are
161 shown in Fig. 4. The incident and transmitter bars, which are 1200 mm in length and
162 14 mm in diameter, are produced with 18Ni steel. The longitudinal wave speed and
163 the Young's modulus of 18Ni steel are 5092 m/s and 210 GPa, respectively. At room
164 temperature, the molybdenum disulfide was adopted between the contact surfaces of
165 the sample and the bars to decrease the friction, and a copper pulse shaper was placed
166 at the impact end of the incident bar to produce a stable wave [33]. A synchronically
167 assembled furnace was designed to heat the sample while keeping the SHPB bars

168 away from it to avoid the influence of elevated temperatures on the bars. The
 169 thermocouple was attached to the sample to measure the sample's temperature.
 170
 171

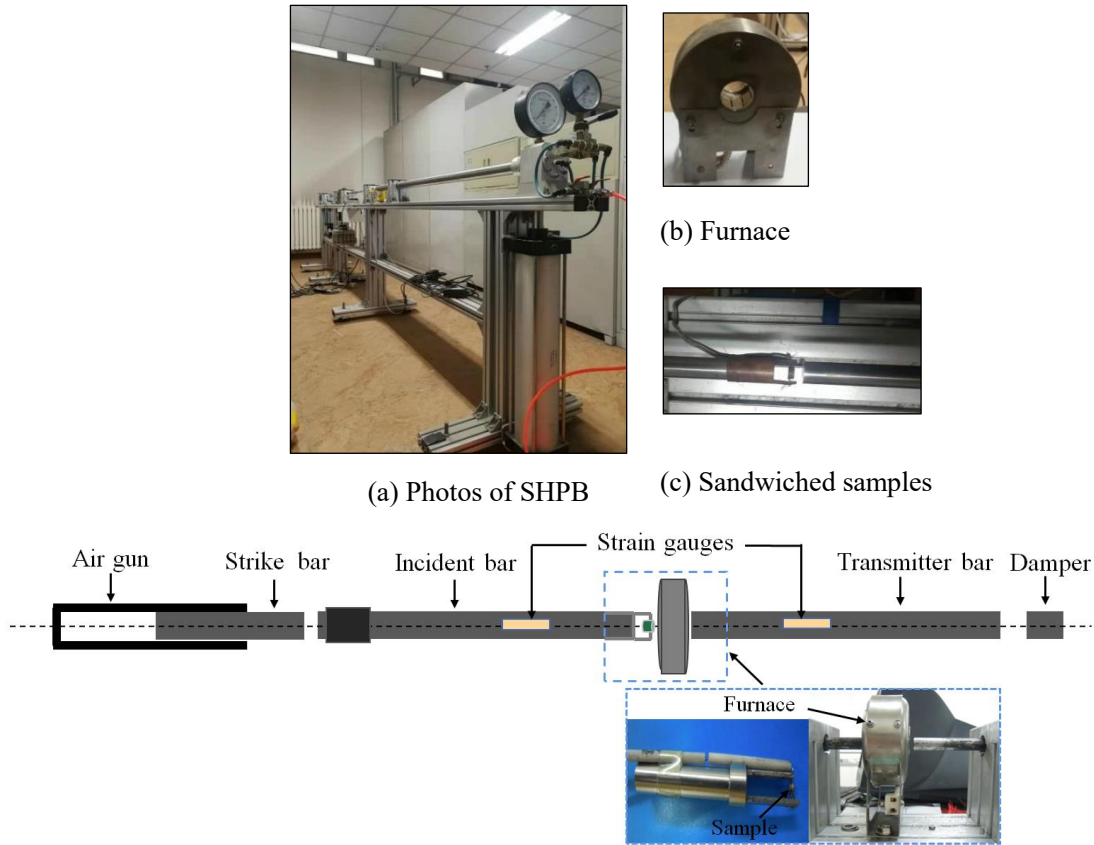


Fig. 4. Set-up for dynamic tests under elevated temperatures.

172 The experiments were performed as follows: (1) Firstly, the samples were mounted
 173 with a thermocouple sleeve and heated at a speed of 2 °C/min to the predetermined
 174 temperature followed by 5 min to achieve a uniform temperature distribution in the
 175 samples; (2) Secondly, the bars were brought into contact with the sample, and then
 176 the strike bar was fired. A similar method was also used in other high-temperature
 177 SHPB test [34]. The incident, transmitter and reflection strain waves (ϵ_I , ϵ_T and ϵ_R)
 178 were detected by the strain gauges. Based on the uniaxial elastic wave theory, the
 179 engineering strain (ϵ_{eng}), engineering stress (σ_{eng}) and strain rate ($\dot{\epsilon}$) can be calculated
 180 by Eqs. (1)-(3), respectively.

$$\varepsilon_{\text{eng}} = -\frac{2C_0}{L} \int_0^t \varepsilon_R dt \quad (1)$$

$$\sigma_{\text{eng}} = E_0 \cdot \frac{A_0}{A_s} \cdot \varepsilon_T \quad (2)$$

$$\dot{\varepsilon} = -\frac{2C_0}{L} \cdot \varepsilon_R \quad (3)$$

181 in which C_0 represents the velocity of the bar elastic wave, A_s and L denote the
 182 cross-sectional area and the gauge length of the sample, respectively; E_0 and A_0
 183 represent the Young's modulus and cross-sectional area of the bars. The true strain
 184 ($\varepsilon_{\text{true}}$) and true stress (σ_{true}) are evaluated as follows:

$$\varepsilon_{\text{true}} = -\ln(1 - \varepsilon_{\text{eng}}) \quad (4)$$

$$\sigma_{\text{true}} = \sigma_{\text{eng}}(1 - \varepsilon_{\text{eng}}) \quad (5)$$

185 The dynamic tests were conducted at temperatures of 20, 200, 400 and 600 °C,
 186 respectively, and averaged strain rates of 1000, 2000 and 3000 s⁻¹. Three samples were
 187 tested at each temperature and strain rate.

188 2.2.3 Microstructure analysis

189 The microstructures of the samples after both elevated temperature and impact
 190 loadings were examined using the optical microscope (Primotech, Zeiss). The samples
 191 were inlaid with a metallographic inlay machine and polished using sandpapers and
 192 polishing machine, and then etched with the aqua regia through repeated wiping.
 193 When the surface colour changes to brown, C₂H₅OH was immediately used to clean
 194 the samples for around 30 s.

195 3. Results and analysis

196 3.1. Stress-strain response

197 As mentioned above, the dynamic stress-strain responses were calculated based on the
 198 strain pulses in the SHPB tests. The typical incident, reflected and transmitted strain
 199 waves (ε_I , ε_R and ε_T) are given in Fig. 5(a). In order to verify the stress equilibrium,
 200 the time histories of $\varepsilon_I + \varepsilon_R$ and ε_T are depicted in Fig. 5(b). As shown, the $\varepsilon_I + \varepsilon_R$
 201 approximately equal to ε_T under dynamic loading, which indicates that the samples
 202 are at a stress equilibrium state and the test results are reliable. It is known that
 203 keeping the strain rate constant is difficult when subjected to the quick loading. In

204 general, the strain rate became relatively stable after experiencing the rapid-rise and
 205 obvious fluctuation stages, and similar trends were also found in other SHPB tests [35,
 206 36]. Given the unstable strain rate over the whole period, the integral averaging
 207 method suggested by Yang et al. [35] is employed to calculate the strain rate in this
 208 work.
 209

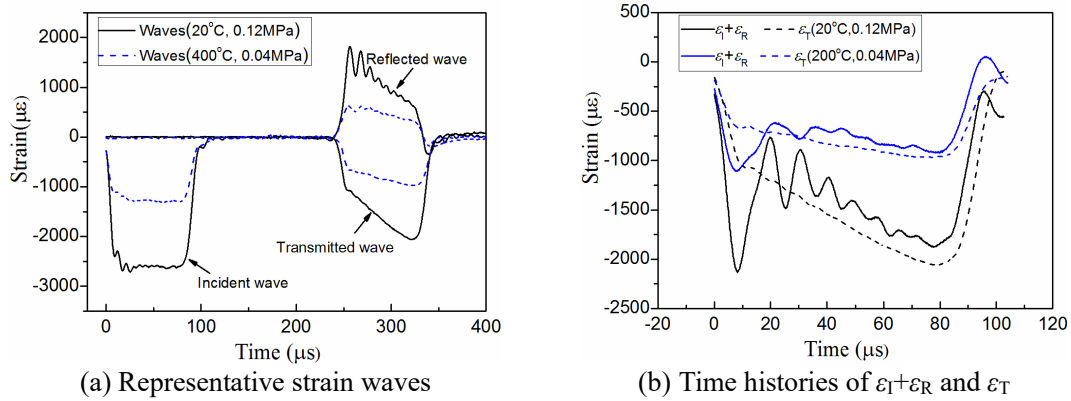
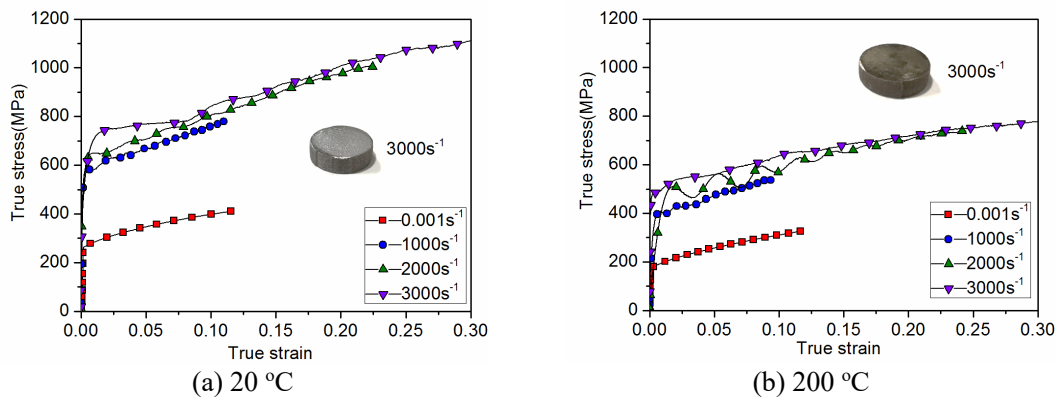


Fig. 5. Typical raw strain waves.

210 Fig. 6 presents the averaged true stress-strain responses of 3 repeated tests deformed
 211 under varying strain rates and temperatures. It is observed that the stress-strain curves
 212 significantly depend on the strain rates and temperatures. The flow stresses rise with
 213 the increasing strain rates, but an increment of temperature results in a decreasing
 214 flow stress. In addition, the stress-strain responses present a work-hardening
 215 behaviour with the increasing strains, and the rate of the working-hardening declines
 216 with an increment of temperature. In the subsequent analysis, the influences of
 217 temperature and strain rate on the yield stresses will be examined.



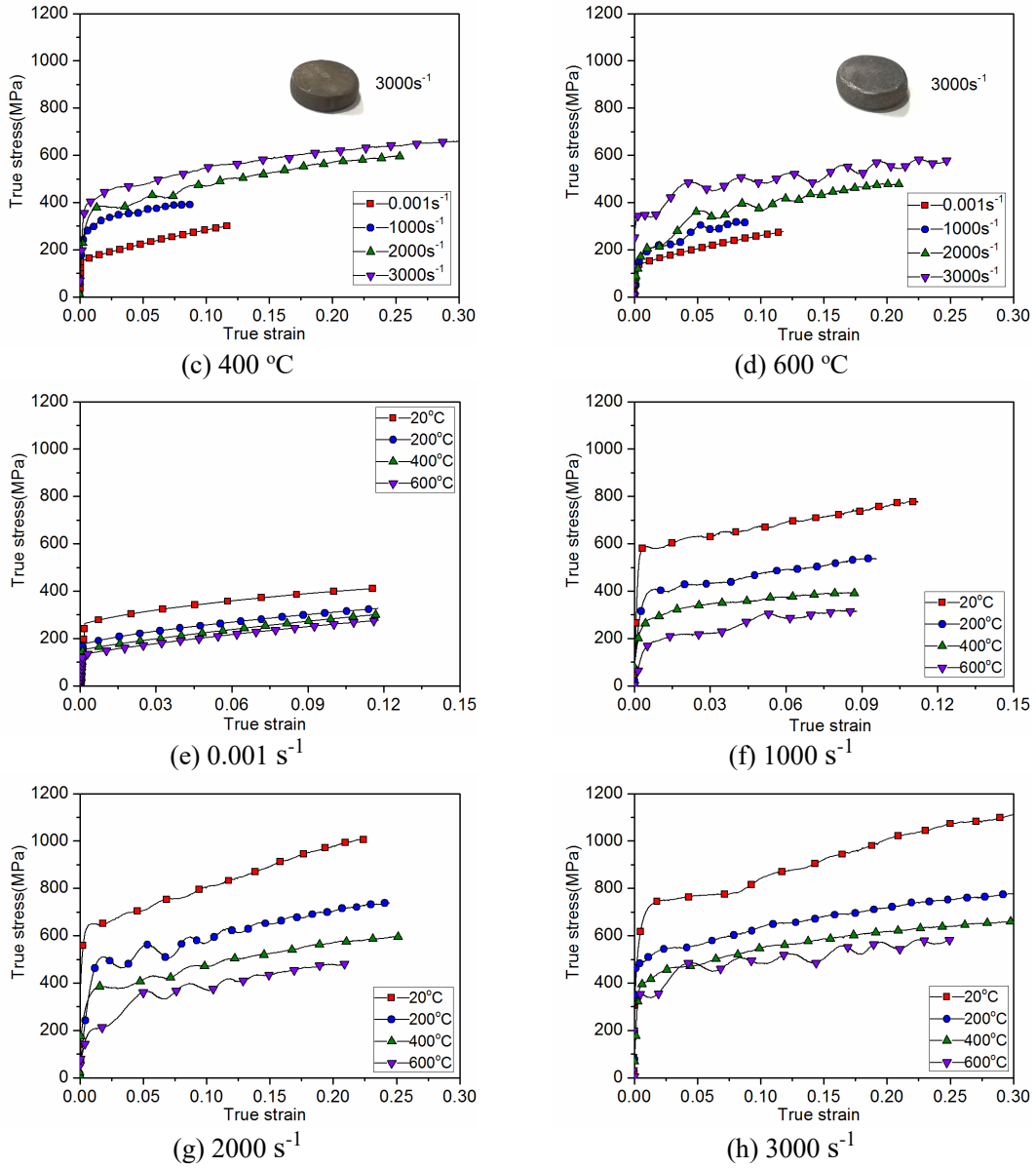
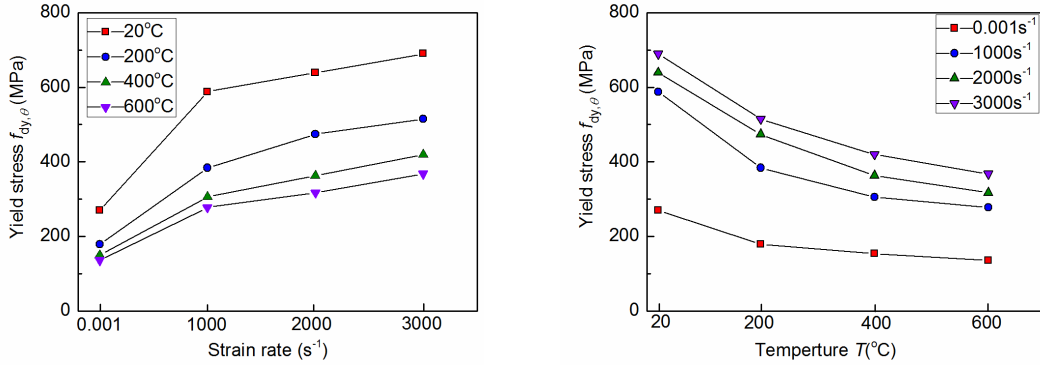


Fig. 6. True stress vs. strain responses.

218 3.2. Influences of strain rate and temperature

219 The variations of yield stresses along with the strain rate and temperature are
 220 presented in Figs. 7(a) and 7(b), respectively. Since the elastic part of the stress-strain
 221 response is fluctuating, the method for extracting the dynamic yield stress is different
 222 from that adopted in the quasi-static test. Thus, the method recommended by Yang et
 223 al. [35] and Sun and Packer [37] was employed to define the dynamic yield stress, as
 224 presented in Fig. 8. It can be seen in Fig. 7 that the yield stresses are sensitive to the
 225 strain rate and temperature. For a given strain rate, the yield stress declines when the
 226 temperature increases. However, it rises with an increment of strain rate when

227 subjected to the same temperature.



(a) Yield stress versus strain rate (b) Yield stress versus temperature
 Fig. 7. Variations of yield stresses with the strain rate and temperature.

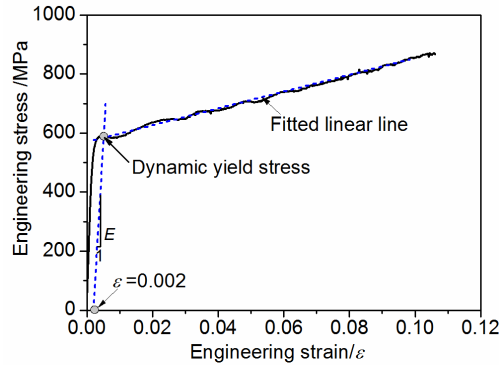


Fig. 8. Definition of dynamic yield stress.

228 In order to quantify influences of strain rate and temperature on the dynamic
 229 compression response, the dynamic increase factor $DIF_{dy,\theta}$ and temperature reduction
 230 coefficient $k_{dy,\theta}$ of the yield stress subjected to varying strain rates and temperatures
 231 are presented in Figs. 9(a) and 9(b), respectively. The corresponding formulas are
 232 given as follows:

$$DIF_{dy,\theta} = f_{dy,\theta} / f_{sy,\theta} \quad (6)$$

$$k_{dy,\theta} = f_{dy,\theta} / f_{dy,20^\circ C} \quad (7)$$

233 in which $f_{dy,\theta}$ and $f_{dy,20^\circ C}$ are the dynamic yield stresses at elevated temperatures and
 234 ambient temperature, respectively; $f_{sy,\theta}$ represent the quasi-static yield stress under
 235 elevated temperatures.

236 The developments of $DIF_{dy,\theta}$ with increasing strain rates under 20, 200, 400 and 600
 237 °C are depicted in Fig. 9(a). As presented, the $DIF_{dy,\theta}$ values under high-strain rates
 238 are greater than 1.0. In general, the highest values appear at 200 °C. The increase rate
 239 of the yield stress from 0.001 to 1000 s^{-1} is higher than that in the range of 1000-2000
 240 s^{-1} and 2000-3000 s^{-1} . For instance, under 400 °C exposure, the yield stresses at strain

241 rates of 1000, 2000 and 3000 s⁻¹ increased by 99%, 136% and 173%, respectively,
 242 compared to that under quasi-static strain rate. It indicates that the strengthening effect
 243 is pronounced under a high strain rate compared with the quasi-static condition. The
 244 evolution of DIF_{dy,θ} in this work is also compared with literature results, as illustrated
 245 in Fig. 9(a). The DIF_{dy,θ} values derived from the results of Lee and Lin [9] are close to
 246 those obtained in this work, while the results of Jia et al. [38] under temperatures of
 247 172 °C are relatively low. The above results indicate that the yield stresses of S30408
 248 ASS present an obvious strain-rate effect.

249 The reduction factors $k_{dy,θ}$ induced by the same temperature were higher under 2000
 250 s⁻¹ and 3000 s⁻¹ than the rest, as presented in Fig. 9(b). There are 2 phases for the yield
 251 strength degradation. The yield strength degrades fastly during 20-200 °C and
 252 gradually decline between 200 °C and 600 °C. When subjected to 200, 400 and 600 °C,
 253 the retained yield strengths under different strain rates are in the range of 65-75%,
 254 52-61% and 47-53% of the values at ambient temperatures, respectively. Fig. 9(b)
 255 also compares the reduction factor of austenitic stainless steel suggested by Fan et al.
 256 [16] and EN 1993-1-2 [23] under the quasi-static loading. These two models are
 257 found to give reasonable predictions of the residual dynamic yield stress under
 258 varying temperatures, considering the variability in high-temperature tests.

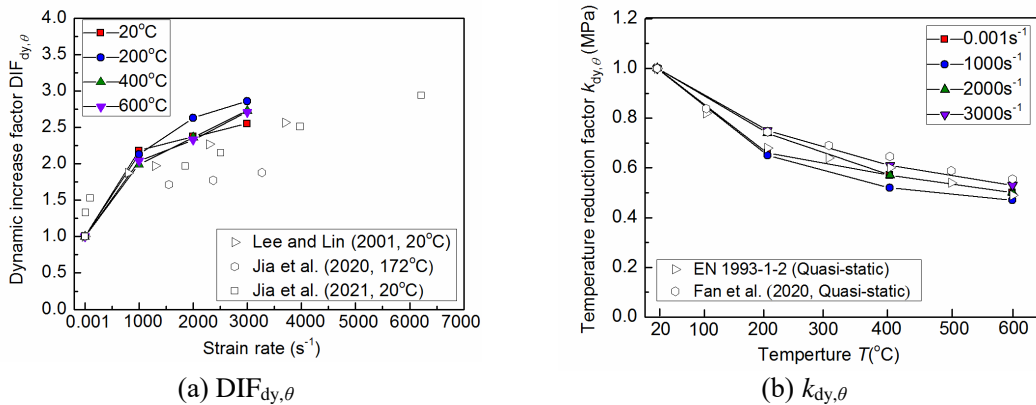


Fig. 9. Dynamic increase factors DIF_{dy,θ} and temperature reduction coefficients $k_{dy,θ}$

259 For each temperature, the influence of the strain rate on the compressive performance
 260 can be qualified via the strain-rate sensitivity coefficient β [18], defined as:

$$\beta = (\ln \sigma_2 - \ln \sigma_1) / (\ln \dot{\epsilon}_2 - \ln \dot{\epsilon}_1) \quad (8)$$

261 in which σ_1 and σ_2 represent the true stresses at 0.05 strain corresponding to the strain

262 rates $\dot{\varepsilon}_1$ and $\dot{\varepsilon}_2$, respectively. The greater value of β indicates more sensitivity to the
 263 strain rate. Fig. 10 presents the variation of parameter β with the strain rate under
 264 different temperatures. The parameter β increases when the strain rate rises, ranging
 265 from 0.03 to 0.4. As the strain rate exceeds 1000 s^{-1} , higher temperature induces the
 266 greater value of β , especially for 400 and 600°C .

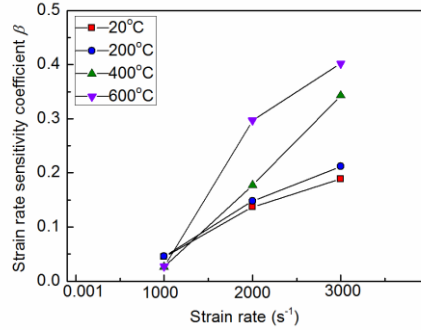


Fig. 10. Strain-rate sensitivity coefficient

267 3.3. Strain rate models

268 Test results have indicated that the stress-strain responses of S30408 ASS are related
 269 to the strain rate and the temperature. Therefore, a widely used temperature and rate
 270 dependence model, called the J-C model [39], is employed to predict the true
 271 stress-strain responses. This model is embedded in the finite element software by
 272 considering the influences of the strain hardening, strain rate strengthening and
 273 temperature softening, which can be written as follows:

$$\sigma = (A + B\varepsilon_p^n) \left(1 + c \ln\left(\frac{\dot{\varepsilon}}{\dot{\varepsilon}_0}\right)\right) (1 - T^{*m}) \quad (9)$$

274 in which ε_p represents the true plastic strain; $\dot{\varepsilon}$ and $\dot{\varepsilon}_0$ are strain rate and quasi-static
 275 strain rate ($=0.001 \text{ s}^{-1}$), respectively; T^* represents the homologous temperature
 276 ($= (T - T_r) / (T_m - T_r)$, T , T_r and T_m denote current temperature, ambient temperature and
 277 melting temperature, respectively); Parameters A , B and n denote the quasi-static
 278 stress-strain response at room temperature; Parameters c and m denote the strain-rate
 279 strengthening and thermal softening effects, respectively. Therefore, these 3 parts in
 280 each bracket are uncoupled in the model.

281 It should be noted that during SHPB tests, a temperature increment occurs due to the
 282 plastic deformation, which is recognized as the adiabatic process. The temperature

283 rise results in the thermal softening and becomes more obvious under higher strain
 284 rate. Thus, the adiabatic temperature increment ΔT is considered in J-C model, as
 285 calculated by Eq.(10):

$$\Delta T = \frac{\beta}{\rho c_p} \int \sigma(\varepsilon) d\varepsilon \quad (10)$$

286 in which β represents the Taylor-Quineey factor taken as 0.9 in this work according to
 287 [26], ρ denotes the density (7.9 g/cm^3), c_p is the heat capacity ($500 \text{ J kg}^{-1}\text{K}^{-1}$).

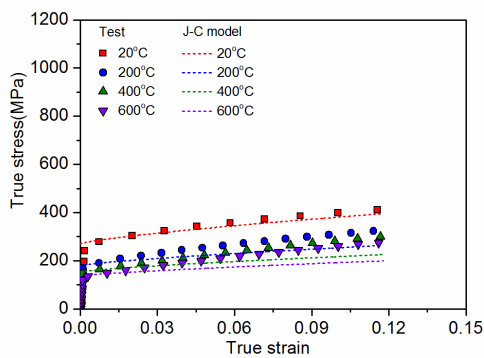
288 By using Eq. (10), taking S30408 ASS under 3000 s^{-1} and $200 \text{ }^\circ\text{C}$ as an example, the
 289 temperature increments achieve $51.5 \text{ }^\circ\text{C}$ at strain of 0.3. Therefore, the temperature
 290 rise caused by the adiabatic process should be incorporated in the model, especially at
 291 higher strain rate.

292 The five parameters are determined by the test results fitting and their values are
 293 presented in Table 2, in which different values of m are given corresponding to
 294 different temperatures. Fig. 11 presents the comparison between the model and test
 295 curves. In general, the model shows a reasonable agreement with the test data. Some
 296 discrepancies between test and predicted results are mainly related to some factors,
 297 such as the microstructural transformation, the adiabatic heat softening and the
 298 experimental error, etc [18, 38, 40].

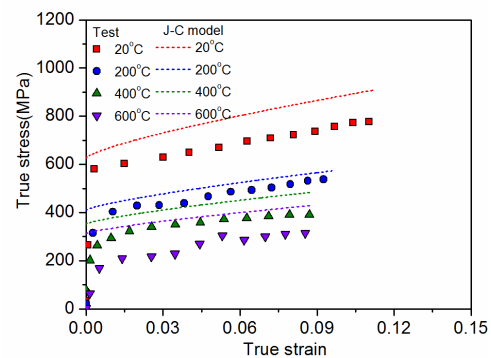
299
 300

Table 2
 Fitted J-C parameters.

$A(\text{MPa})$	$B(\text{MPa})$	n	c	m		
				200°C	400°C	600°C
270	637	0.7587	0.0959	0.538	0.653	0.808



(a) 0.001 s^{-1}



(b) 1000 s^{-1}

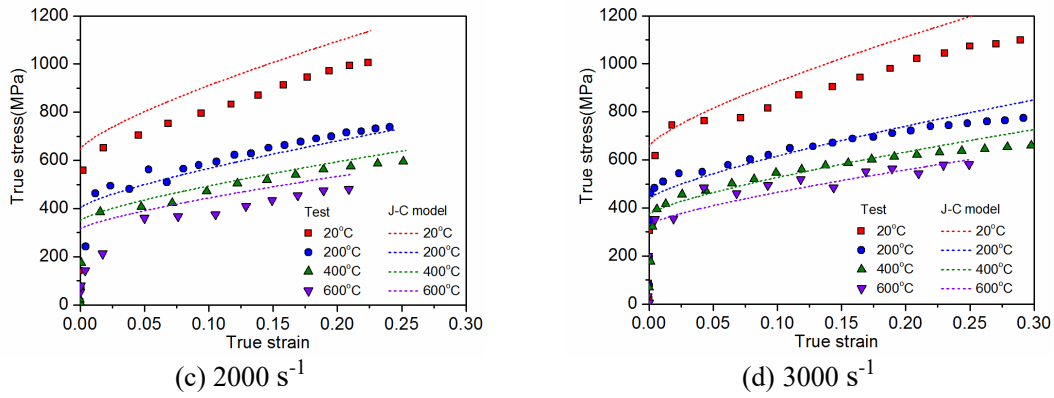
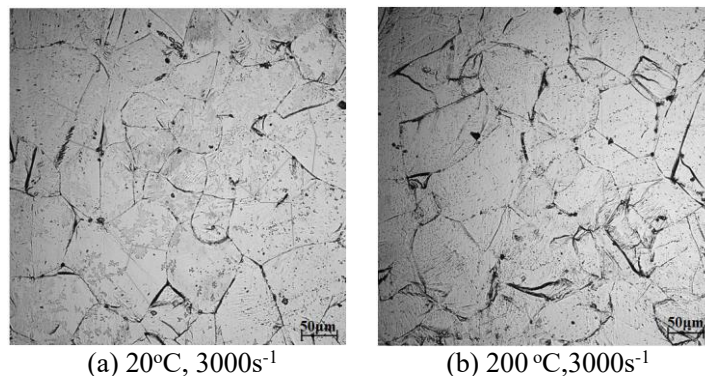


Fig. 11. Comparison between the test results and J-C model

301 **3.4. Microstructural observation after elevated-temperature dynamic test**

302 After compression deformation, the microstructures were examined using the optical
 303 microscopy to analyze the relationship between the elevated-temperature dynamic
 304 properties and the residual microstructure, as presented in Fig. 12. The photographs
 305 show that a higher temperature results in a pronounced increase in the grain sizes and
 306 a decline of the grain boundary area when exposed to the same strain rate.
 307 Considering that the grain boundary hinders the plastic deformation and has higher
 308 strength than the inner grain, the smaller the grain boundary area is, the lower the
 309 strength and hardness are. Therefore, the inferior mechanical responses of S30408
 310 ASS were obtained at higher temperatures. In addition, as the strain rate increases, the
 311 average grain dimension decreases while the grain boundary gradually diffuses and
 312 become irregular. Therefore, the rise in the grain boundary area under a higher strain
 313 rate benefits the mechanical performance. In general, the grains maintain a well
 314 integrity structure, and the changes in the grain shape are unobvious under varying
 315 temperatures and strain rates, indicating a good performance of S30408 ASS under
 316 coupled fire and impact loadings.



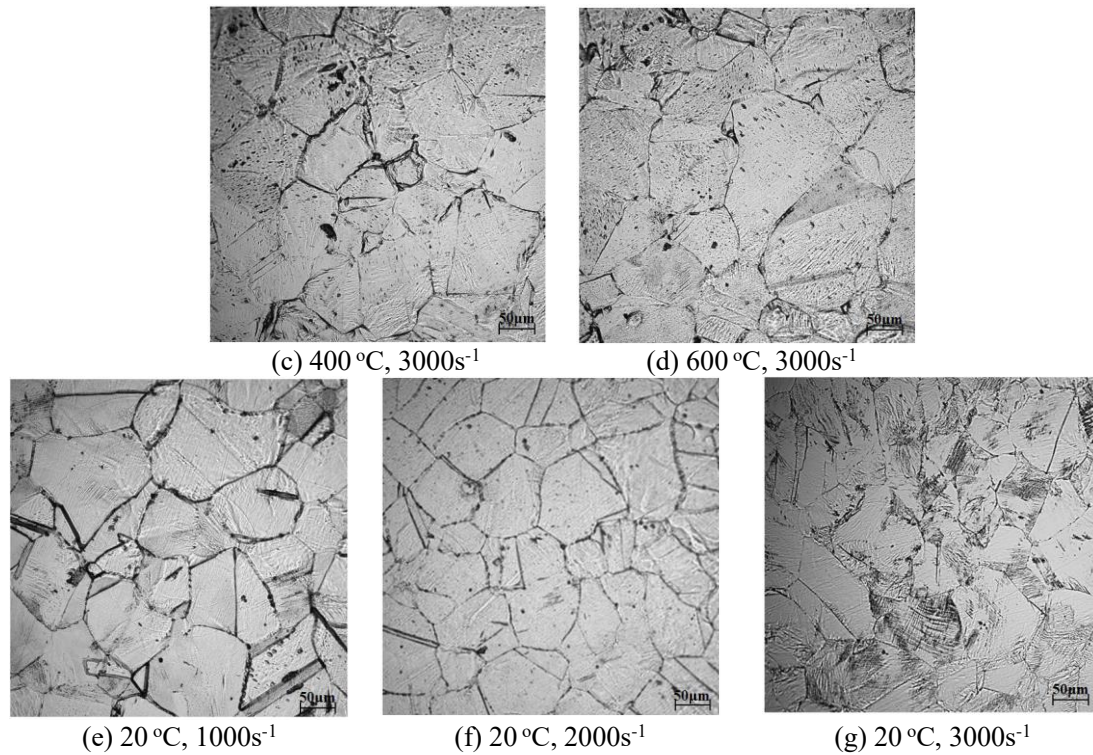


Fig. 12. Optical microstructures under different strain rates and temperatures.

317 4. Conclusions

318 This study investigated the quasi-static and dynamic compressive behaviours of
 319 S30408 austenitic stainless steel (ASS) under elevated temperatures of 20, 200, 400
 320 and 600 °C and strain rates ranged from 0.001 s⁻¹ to 3000 s⁻¹. According to the test and
 321 analyses, the main conclusions are obtained:

322 (1) The compressive responses of S30408 ASS are sensitive to the strain rate and
 323 temperature. The yield stress increases with an increment of the strain rate, but
 324 declines with increased temperatures. In addition, the rate of the working-hardening
 325 becomes weaker at higher temperatures.

326 (2) As the strain rate rises from 0.001 s⁻¹ to 3000 s⁻¹, the elevated-temperature
 327 dynamic increase factors $DIF_{dy,\theta}$ rises, with the maximum value of 2.86 under 200 °C
 328 and 3000 s⁻¹. The temperature reduction coefficients $k_{dy,\theta}$ decreases significantly
 329 during 20-200 °C and the reduction slows down from 200 to 600 °C. The strain-rate
 330 sensitivity coefficient is more pronounced under a higher strain rate and a higher
 331 temperature.

332 (3) Based on the experimental results, the parameters for J-C constitutive model were

333 determined. This model could be used to predict the residual performance of
334 structures made with this type of steel under the coupled action of fire and
335 impact/blast loadings.

336 (4) Residual microstructure indicates that higher temperatures result in an obvious rise
337 of the grain size, while the increase in the strain rate decreases the grain size. In
338 general, the moderate grain deformation occurs under coupled high temperatures and
339 strain rates within the parameter range in this work.

340 **Acknowledgements**

341 The study was supported by the China Postdoctoral Science Foundation
342 (2020M670656) and Fund Program for the Scientific Activities of Selected Returned
343 Overseas Professionals in Shanxi Province (20210010).

344 **References**

- 345 [1] L.H. Han, C.Y. Xu, Z. Tao, Performance of concrete filled stainless steel tubular (CFSST)
346 columns and joints: Summary of recent research, *J. Constr. Steel Res.* 152 (2019) 117-131.
- 347 [2] H. Zhao, R Wang, C.C. Hou, D. Lam, Performance of circular CFDST members with external
348 stainless steel tube under transverse impact loading, *Thin-Walled Struct.* 145 (2019) 106380.
- 349 [3] S.K. Azad, D.X. Li, B. Uy, Axial slenderness limits for austenitic stainless steel-concrete
350 composite columns, *J. Constr. Steel Res.* 166 (2020) 105856.
- 351 [4] M. Kucukler, Z. Xing, L. Gardner, Behaviour and design of stainless steel I-section columns
352 in fire, *J. Constr. Steel Res.* 165 (2020) 105890.
- 353 [5] I. Arrayago, K.J.R. Rasmussen, E. Real, Statistical analysis of the material, geometrical and
354 imperfection characteristics of structural stainless steels and members, *J. Constr. Steel Res.*
355 175 (2020) 106378.
- 356 [6] H. Zhao, R Wang, D. Lam, C.C. Hou, R Zhang, Behaviours of circular CFDST with stainless
357 steel external tube: Slender columns and beams, *Thin-Walled Struct.* 158 (2021) 107172.
- 358 [7] CECS 410: 2015, Technical Specification for Stainless Steel Structure, Planning Press of

359 China, Beijing, 2015 (In Chinese).

360 [8] EN 1993-1-4:2006+A1: 2015. Eurocode 3—Design of Steel Structures Part1—4: General
361 Rules-Supplementary Rules for Stainless Steel. British Standards Institution. London, UK,
362 2015.

363 [9] W.S. Lee, C.F. Lin, Impact properties and microstructure evolution of 304L stainless steel,
364 Mater. Sci. Eng. A. 308(2001) 124-135.

365 [10]J.A. Lichtenfeld, C.J.V. Tyne, M.C. Mataya, Effect of strain rate on stress-strain behavior of
366 alloy 309 and 304L austenitic stainless steel, Metall. Mater. Trans. A. 37 (2006) 147-161.

367 [11]F. Zhou, B. Young, Experimental and numerical investigations of cold-formed stainless steel
368 tubular sections subjected to concentrated bearing load, J. Constr. Steel Res. 63(11)(2007)
369 1452-1466.

370 [12]K. Abdella, Explicit full-range stress-strain relations for stainless steel at high temperatures, J.
371 Constr. Steel Res. 65 (2009) 794-800.

372 [13]E. Cadoni, L. Fenu, D. Forni, Strain rate behaviour in tension of austenitic stainless steel used
373 for reinforcing bars, Constr. Build. Mater. 35 (2012) 399-407.

374 [14]F. Zhou, L. Li, Experimental study on hysteretic behavior of structural stainless steels under
375 cyclic loading, J. Constr. Steel Res. 122(2016) 94-109.

376 [15]M.J. Liu, S.G. Fan, R.M. Ding, G.Q. Chen, E.F. Du, K. Wang, Experimental investigation on
377 the fire resistance of restrained stainless steel H-section columns, J. Constr. Steel Res.
378 163(2019) 105770.

379 [16]S.G. Fan, R.M. Ding, J.C. Zheng, F.Z. Xie, Refined model for the stress-strain curve of
380 austenitic stainless-steel materials at elevated temperatures, J. Mater. Civ. Eng. 32 (4) (2020)
381 04020032.

382 [17]D. Fernando, J.G. Teng, W.M. Quach, L.D. Waal, Full-range stress-strain model for stainless
383 steel alloys, J. Constr. Steel Res. 173(2020) 106266.

384 [18]S.G. Jia, Q.H. Tan, J.Y. Ye, Z.W. Zhu, Z.G. Jiang, Experiments on dynamic mechanical
385 properties of austenitic stainless steel S30408 and S31608, J. Constr. Steel Res. 179(2021)
386 106556.

- 387 [19]A.D. Martins, R. Gonçalves, D. Camotim, Numerical simulation and design of stainless steel
388 columns under fire conditions, *Eng. Struct.* 229(2021) 111628.
- 389 [20]H.X. Yuan, X.H. Liu, J.L. Liu, M. Theofanous, Cyclic behaviour and hysteretic model of
390 austenitic stainless steel bolted T-stubs, *J. Constr. Steel Res.* 182 (2021) 106659.
- 391 [21]D. Forni, B. Chiaia, E. Cadoni, High strain rate response of S355 at high temperatures, *Mater.*
392 *Des.* 94(2016) 467-478.
- 393 [22]E. Cadoni, D. Forni, Mechanical behaviour of a very-high strength steel (S960QL) under
394 extreme conditions of high strain rates and elevated temperatures, *Fire Saf. J.* 109(2019)
395 102869.
- 396 [23]BS EN 1993-1-2, Eurocode 3: Design of steel structures: Part 1-2: General rules-Structural
397 fire design, BSI, London, 2005.
- 398 [24]W.S. Lee, C.F. Lin, T.H. Chen, M.C. Yang, High temperature microstructural evolution of
399 304L stainless steel as function of pre-strain and strain rate, *Mater. Sci. Eng. A.* 527(2010)
400 3127-3137.
- 401 [25]W.S. Lee, C.F. Lin, T.H. Chen, M.C. Yang, Effects of prestrain on high temperature impact
402 properties of 304L stainless steel, *J. Mater. Res.* 25(4)(2010) 754-762.
- 403 [26]E. Cadoni, D. Forni, Austenitic stainless steel under extreme combined conditions of loading
404 and temperature, *J. Dynamic Behav. Mater.* 5(3)(2019) 230-240.
- 405 [27]Q.S. Yan, C.X. Lv, B.W. Sun, L. Yang, Dynamic mechanical behavior at elevated
406 temperatures and high strain rate of structural stainless steel used in civil engineering, *J. Mater.*
407 *Civ. Eng.* 32 (5) (2020) 04020094.
- 408 [28] A1022/A1022M-16b, Standard specification for deformed and plain stainless steel wire and
409 welded wire for concrete reinforcement. ASTM International, United States, 2016.
- 410 [29] EN 10088-1: 2014, Stainless steels-Part 1: List of stainless steels, European committee for
411 standardization, Brussels, 2014.
- 412 [30]EN ISO 377:2013, Steel and steel products - location and preparation of samples and test
413 pieces for mechanical testing, CEN, Brussels, 2013.
- 414 [31]GB/T 228.1-2010, Metallic materials-Tensile testing-Part 1 Method of test at room

415 temperature. China Architecture & Building Press, Beijing, China, 2010.

416 [32]GB/T 34108-2017, Code for metallic materials-high strain rate compression method at
417 ambient temperature, Standards Press of China, Beijing, China, 2017.

418 [33]Y.X. Mei, H.Y. Ban, High strain rate behaviour of stainless-clad bimetallic steel, *Eng. Struct.*
419 207(2020) 110219.

420 [34] P. Ponnusamy, S.H. Masooda, D. Ruan, S. Palanisamy, R.A.R. Rashid, R. Mukhlis, N.J.
421 Edwards, Dynamic compressive behaviour of selective laser melted AlSi12 alloy: Effect of
422 elevated temperature and heat treatment, *Addit. Manuf.* 36 (2020) 101614.

423 [35]X.Q. Yang, H. Yang, S.M. Zhang, Rate-dependent constitutive model of S690 high-strength
424 structural steel, *Constr. Build. Mater.* 198 (2019) 597-607.

425 [36]Y. Zhu, H. Yang, S.M. Zhang, Dynamic mechanical behavior and constitutive models of S890
426 high-strength steel at intermediate and high strain rates, *J. Mater. Eng. Perform.* 29(2020)
427 6727-6739.

428 [37]M. Sun, J.A. Packer, High strain rate behavior of cold-formed rectangular hollow sections,
429 *Eng. Struct.* 62(2014) 181-192.

430 [38]B. Jia, A. Rusinek, R. Pesci, S. Bahi, R. Bernier, Thermo-viscoplastic behavior of 304
431 austenitic stainless steel at various strain rates and temperatures: Testing, modeling and
432 validation, *Int. J. Mech. Sci.* 170(2020) 105356.

433 [39]G.R. Johnson, W.H. Cook, A constitutive model and data for metals subjected to large strains,
434 high strain rates and high temperatures, Den Haag, The Netherlands Proceedings of the 7th
435 International Symposium on Ballistics (1983), pp. 541-547.

436 [40]X.L. Fan, T. Suo, Q. Sun, T.J. Wang, Dynamic mechanical behavior of 6061 AL alloy at
437 elevated temperatures and different strain rates, *Acta Mech. Solida Sin.* 26(2013) 111-120.